J. Fluid Mech. (2023), *vol.* 958, A35, doi:10.1017/jfm.2023.124

Scaling maximum spreading of droplet impacting on flexible substrates

Yufei Ma[1] **and Haibo Huang**[1],†

[1]Department of Modern Mechanics, University of Science and Technology of China, Hefei, Anhui 230026, PR China

(Received 29 March 2022; revised 4 February 2023; accepted 4 February 2023)

We numerically study the impact of a droplet on superhydrophobic flexible plates, aiming to understand how the flexible substrate influences the maximum spreading of the droplet. Compared with the rigid case, the vertical movement of the flexible substrate due to droplet impact reduces the maximum spreading. Besides, the average acceleration a during droplet spreading changes significantly. Arising from energy conservation, we rescale the acceleration a for cases with different bending stiffness K_B and mass ratio M_r. Moreover, through theoretical analysis, we propose a scaling for the droplet's maximum spreading diameter ratio β_{max}. In the scaling, based on the derived a, an effective Weber number We_m is well defined, which accounts for the substrate properties without any adjustable parameters. In the (β_{max}, We_m) plane, the two-dimensional numerical results of different K_B, M_r and rigid cases all collapse into a single curve, as do the experimental and three-dimensional (3-D) results. In particular, the collapsed 3-D data can be well represented by the universal rescaling of β_{max} proposed by Lee *et al.* (*J. Fluid Mech.*, vol. 786, 2016, R4). Furthermore, an *a posteriori* energy analysis confirms the validation of our *a priori* scaling law.

Key words: flow–structure interactions, drops, contact lines

1. Introduction

The impact of a liquid droplet on a solid surface is ubiquitous. It occurs in nature, industry and agriculture, such as raindrop impact on soil (Joung & Buie 2015), inkjet printing (Derby 2010) and pesticide deposition on plant leaves (Bergeron *et al.* 2000). During the impacting, droplets can spread, rebound or splash, depending on viscosity, surface tension, impact velocity and the properties of the solid surface (Josserand & Thoroddsen 2016). The maximum spreading of droplets is relevant to the inertia, surface tension and viscosity and, thus, involves two important dimensionless parameters: the Weber number

† Email address for correspondence: huanghb@ustc.edu.cn

$We = \rho_H U_0^2 D_0/\sigma$ and the Reynolds number $Re = \rho_H U_0 D_0/\mu_H$, where U_0 is the initial impact velocity, D_0 is the initial droplet diameter, σ is the surface tension coefficient, ρ_H is the liquid density and μ_H is the dynamic viscosity.

At present, many theoretical models based on energy or momentum conservation have been proposed to predict the maximum spreading diameter ratio $\beta_{max} = D_{max}/D_0$ of droplets impacting on a solid surface. In the literature, four scalings have been proposed to balance capillary, viscous and inertial forces. These include $\beta_{max} \sim Re^{1/4}$ (Pasandideh-Fard *et al.* 1996) and $\beta_{max} \sim Re^{1/5}$ (Roisman 2009; Wildeman *et al.* 2016) to balance viscous and inertial forces, and $\beta_{max} \sim We^{1/2}$ (Eggers *et al.* 2010) and $\beta_{max} \sim We^{1/4}$ (Clanet *et al.* 2004) to balance capillary and inertial forces. However, the $We^{1/4}$ scaling may not be correct (Laan *et al.* 2014) due to the balance being performed in a non-Galilean frame of reference in Clanet *et al.* (2004). Laan *et al.* (2014) believed that all three forces play an important role when We and Re have similar values. They proposed a new scaling combining $Re^{1/5}$ and $We^{1/2}$, which is in good agreement with the experimental results. Besides, they found that the data points could not be collapsed onto one single curve using the scaling of $We^{1/4}$, suggesting that $We^{1/4}$ is not correct. Later, Lee *et al.* (2016) further took the wettability and roughness of solid surfaces into account, and proposed a universal rescaling of the β_{max} for different liquids and surfaces. As for nanodroplets, the scaling laws of $\beta_{max} \sim We^{1/5}$ and $We^{2/3}Re^{-1/3}$ in low and high We regimes, respectively, was proposed by Wang *et al.* (2022).

The studies above are all about a droplet impacting on the rigid substrate, while there are few studies considering flexible substrates. According to previous studies, the flexible substrate also has a great influence on droplet impact. For superhydrophobic flexible substrates, Weisensee *et al.* (2016) experimentally found that part of the momentum is returned to the droplet through the substrate's vertical vibration, resulting in a reduction of the contact time. Howland *et al.* (2016) experimentally found that the energy consumption due to the deformation of the flexible substrate can reduce or suppress the splashing of droplets. While Pegg, Purvis & Korobkin (2018) found that the vibration of the flexible substrate is one of the key factors leading to splash through theoretical and numerical analysis. Vasileiou *et al.* (2016) experimentally found that the flexible substrate can enhance the superhydrophobicity of the solid surface, which is characterized by larger impalement resistance, smaller β_{max} and shorter contact time of droplet impact. Besides, this problem has been widely studied involving the raindrop impacting on biological surfaces (Gart *et al.* 2015; Kim *et al.* 2020).

Although there are some qualitative experimental investigations, there are few quantitative analyses on the maximum spreading of droplets impacting flexible substrates. As far as we know, only Vasileiou *et al.* (2016) and Xiong, Huang & Lu (2020) tried to perform quantitative analyses. However, Vasileiou *et al.* (2016) only considered the influence of the mass ratio of the droplet to the flexible plate, and the effect of the bending stiffness for plates was ignored. Xiong *et al.* (2020) used the same methods as this work to perform relevant simulations. However, Xiong *et al.* (2020) only focused on the two-dimensional (2-D) spreading dynamics in a very limited We range at a fixed mass ratio M_r. Furthermore, the final results were not normalized well.

In this paper a droplet impacting flexible plates over a wide range of We (0.1–100) in both two and three dimensions is simulated and quantitative analyses are carried out. Not only the effect of the stiffness K_B of the flexible plate but also that of the mass ratio M_r on the maximum spreading are investigated. Besides, the corresponding inherent mechanism is explored. We aim to seek a universal scaling law of β_{max} in this flow problem.

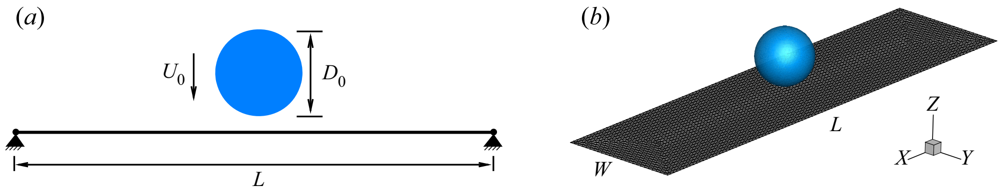

Figure 1. (*a*) The physical problem (two dimensional). (*b*) The three-dimensional (3-D) case. Here, W is the width of the plate.

2. Methodology and validation

A schematic diagram about a droplet impacting on a flexible plate is shown in figure 1(*a*). The droplet with a diameter D_0 has a downwards impact velocity U_0. It is initially set above the centre of the flexible plate. The initial length of the plate is L and the two ends of the plate are simply supported. Figure 1(*b*) shows the three-dimensional (3-D) viewpoint. Here, in our simulations, the phase-field lattice Boltzmann method (LBM) (Liang *et al.* 2018) and the finite element method (Doyle 2001) are adopted for solving the fluid flow and the solid deformation, respectively. The conservative phase-field equation (Allen–Cahn equation) is used to track the fluid interface (Xiong *et al.* 2020)

$$\frac{\partial \phi}{\partial t} + \nabla \cdot (\phi \boldsymbol{u}) = \nabla \cdot \left[M \left(\nabla \phi - \frac{4}{\xi} \phi (1-\phi) \hat{\boldsymbol{n}} \right) \right], \tag{2.1}$$

where ϕ is the component variable varying from 0 to 1, corresponding to light (vapour) and heavy (liquid) fluids, respectively. The densities of light and heavy fluids are ρ_L and ρ_H, respectively. Here, $\boldsymbol{u}$ is the macroscopic velocity vector, M is the mobility, ξ is the interface thickness and $\hat{\boldsymbol{n}}$ is the unit vector normal to the fluid interface as $\nabla\phi/|\nabla\phi|$, pointing to the liquid. The isothermal, incompressible Navier–Stokes equation is solved by the LBM. The motion and deformation of the flexible plate for 2-D and 3-D cases are described by the structural equations (2.2) and (2.3), respectively (Hua, Zhu & Lu 2014; Xiong *et al.* 2020), i.e.

$$\rho_s h_s \frac{\partial^2 \boldsymbol{X}}{\partial t^2} - \frac{\partial}{\partial s}\left[Eh_s \left(1 - \left| \frac{\partial \boldsymbol{X}}{\partial s} \right|^{-1} \right) \frac{\partial \boldsymbol{X}}{\partial s} \right] + EI \frac{\partial^4 \boldsymbol{X}}{\partial^4 s} = \boldsymbol{F}_{ext}, \quad 2D, \tag{2.2}$$

$$\rho_s h_s \frac{\partial^2 \boldsymbol{X}}{\partial t^2} - \sum_{i,j=1}^{2} \left[\frac{\partial}{\partial s_i} \left(Eh_s \varphi_{ij} \left[\delta_{ij} - \left(\frac{\partial \boldsymbol{X}}{\partial s_i} \cdot \frac{\partial \boldsymbol{X}}{\partial s_j} \right)^{-1/2} \right] \frac{\partial \boldsymbol{X}}{\partial s_j} - \frac{\partial}{\partial s_j} \left(EI \gamma_{ij} \frac{\partial^2 \boldsymbol{X}}{\partial s_i \partial s_j} \right) \right) \right] = \boldsymbol{F}_{ext}, \quad 3D, \tag{2.3}$$

where s is the Lagrangian coordinate along the plate direction, $\boldsymbol{X}$ is the position vector of the plate, ρ_s is the plate density, h_s is the plate thickness, EI and Eh_s are the bending and stretching stiffnesses, respectively, where $I = h_s^3/12$ and E is Young's modulus. Here, φ_{ij} and γ_{ij} are the in-plane and out-of-plane effect matrices, respectively, and their components are $\varphi_{11} = \varphi_{22} = 1$, $\varphi_{12} = \varphi_{21} = 1/(2+2\nu)$, $\gamma_{11} = \gamma_{22} = 1$ and $\gamma_{12} = \gamma_{21} = 0$, where ν is Poisson's ratio. We denote by δ_{ij} the Kronecker delta function and $\boldsymbol{F}_{ext}$ the external force exerted by the fluid on the plate. The initial plate is straight, i.e. $(\partial^2 \boldsymbol{X}^0/\partial s_i^2 \cdot \partial^2 \boldsymbol{X}^0/\partial s_j^2)^{1/2} = 0$ and the initial tension is zero, i.e. $(\partial \boldsymbol{X}^0/\partial s_i \cdot \partial \boldsymbol{X}^0/\partial s_j)^{1/2} = \delta_{ij}$, where $\boldsymbol{X}^0$ is the initial position vector.

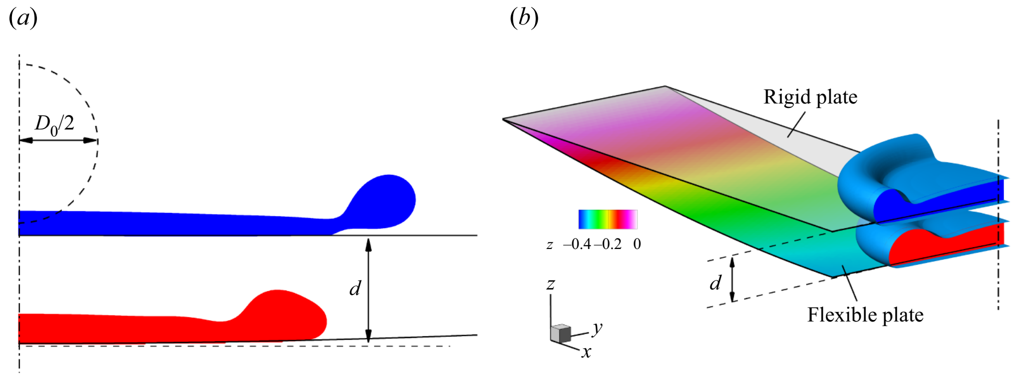

Figure 2. Snapshots of impacting droplets at the maximum spreading with $We = 60$ for rigid (blue) and flexible (red, $K_B = 1.0$ and $M_r = 0.01$) cases. In (*a*) the 2-D and (*b*) the 3-D cases, half and a quarter of the droplets are shown, respectively. Here, d is the deflection of the plate at the centre. For the 3-D flexible case, on the plate, the contours of deflection in the z direction are shown.

Due to the symmetry of this problem, the following techniques are applied to save CPU time. In the 2-D cases, by applying a symmetric boundary condition, our computational domain is only half of the entire domain of the physical problem (see figure 2*a*). Similarly, for the 3-D cases, by applying the symmetric boundary conditions, our computational domain is only a quarter of the entire domain of the physical problem (see figure 2*b*). Here, the momentum exchange method is adopted for the moving boundary. Except for the symmetric boundaries, the outflow boundary conditions are applied for the other boundaries. As for the wettability of the substrate, the following Neumann boundary condition (Shao, Shu & Chew 2013; Fakhari & Bolster 2017) is applied to impose the static contact angle:

$$\hat{n}_w \cdot \nabla\phi|_w = \Theta\phi_w(1-\phi_w). \tag{2.4}$$

Here, $\hat{n}_w$ is the unit vector normal to the solid boundary and ϕ_w is the component variable at the boundary point; Θ is related to the equilibrium contact angle θ, i.e. $\Theta = -\sqrt{2\alpha/\kappa}cos\theta$, where α and κ are related to the surface tension σ and the interfacial thickness ξ by $\alpha = 12\sigma/\xi$ and $\kappa = 3\sigma\xi/2$; ϕ_w and $\nabla\phi|_w$ can be calculated from the values of ϕ in the surrounding nodes. To improve the accuracy, a weighted least squares method is adopted (Pan, Ni & Zhang 2018). More details about the implementation of this numerical method can be found in Xiong *et al.* (2020).

To make the above equations dimensionless, we choose ρ_H, D_0 and σ as characteristic quantities. The corresponding reference speed and time are $U_{ref} = \sqrt{\sigma/(\rho_H D_0)}$ and $T_{ref} = \sqrt{\rho_H D_0^3/\sigma}$, respectively. The key dimensionless parameters in the problem are the Weber number $We = \rho_H U_0^2 D_0/\sigma$, the bending stiffness $K_B = EI/(\rho_H U_{ref}^2 L^3)$ and the mass ratio $M_r = \rho_s h_s/(\rho_H L)$. Here, in our simulations, the density ratio is $\rho_H/\rho_L = 1000$, the dynamic viscosity ratio $\mu_H/\mu_L = 50$, the Ohnesorge number $Oh = \sqrt{We}/Re = 0.01$, the contact angle $\theta = 170^\circ$, the stretching stiffness $K_S = Eh_s/(\rho_H U_{ref}^2 L) = 100$, the length ratio $L/D_0 = 20$ in 2-D cases, and $L/D_0 = 8$, the width ratio $W/D_0 = 3$ in 3-D cases. Because our numerical methods have been quantitatively validated in our previous work for the 2-D case (Xiong *et al.* 2020), here we mainly carried out validations for 3-D cases. The cases for droplets impacting on rigid substrates were simulated. Through the grid-independence study with different resolutions ($D_0 = 150\Delta x$, $300\Delta x$ and $600\Delta x$),

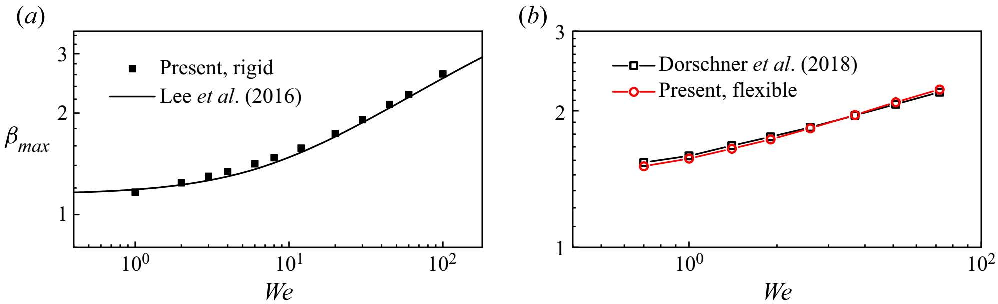

Figure 3. The β_{max} as a function of We for (*a*) a rigid substrate, where the black squares represent our 3-D simulation results, and the solid line denotes the scaling of Lee *et al.* (2016). (*b*) Results for a flexible substrate, where the red and black symbols denote our results and those from Dorschner, Chikatamarla & Karlin (2018), respectively.

we found that $D_0 = 300\Delta x$ is sufficient to obtain accurate results (not shown) and in the following simulations the resolution is adopted. In all of our 2-D and 3-D calculations, the computational domains are $10D_0 \times 3D_0$ and $4D_0 \times 1.5D_0 \times 3D_0$ with a uniform Cartesian mesh, respectively.

Our numerical results, shown in figure 3(*a*), demonstrate good agreement with the universal rescaling of β_{max} proposed by Lee *et al.* (2016) for rigid cases. It is important to note that this rescaling depends not only on We but also on Re. In line with this, all of our simulations were conducted with $Oh = \sqrt{We}/Re = 0.01$, which means that Re varied with We. Furthermore, our results for flexible cases also agree well with the numerical results of Dorschner *et al.* (2018) in figure 3(*b*). Therefore, our numerical method for the simulations of a droplet impacting flexible plates is validated.

3. Results and discussion

The droplet impacting on the flexible substrate would lead to a vertical movement of the substrate, which may affect the spreading of the droplet in turn. During this coupling process, the parameters, such as We, K_B and M_r, are all important. Here, we focus on their influences on the maximum spreading. A series of simulations in a wide range of parameters were performed, specifically, $We \in [0.1, 100]$, $K_B \in [0.01, \infty)$ and $M_r \in [0.006, \infty)$. It is noted that the cases of $K_B = \infty$ and $M_r = \infty$ correspond to the rigid case.

The results of the maximum spreading diameter ratio β_{max} as a function of We are shown in figure 4. It can be seen from figure 4(*a*,*c*) that when M_r is fixed, the maximum spreading D_{max} is reduced as K_B decreases at a specific We in both 2-D and 3-D simulations. It can be simply described as 'flexibility reduces spreading'. Similarly, when K_B is fixed, the spreading is enhanced as M_r increases. It can be understood as follows. When the inertia of the plate is relatively large (large M_r), it is hard to move and oscillate even if there is an impact from the droplet. The situation is similar to the rigid case. Therefore, the trend can be simply described as 'inertia of plate enhances spreading'. A more detailed analysis about these can be seen in § 3.1.

From figure 4 we can see that the trends of the simulation results for the 2-D and 3-D cases are similar. It can be understood in the following way. First, there is an inherent connection between the 2-D and 3-D substrate equations. The substrate equation for 3-D cases, i.e. (2.3), can degenerate into the 2-D equation, i.e. (2.2), if the spanwise length

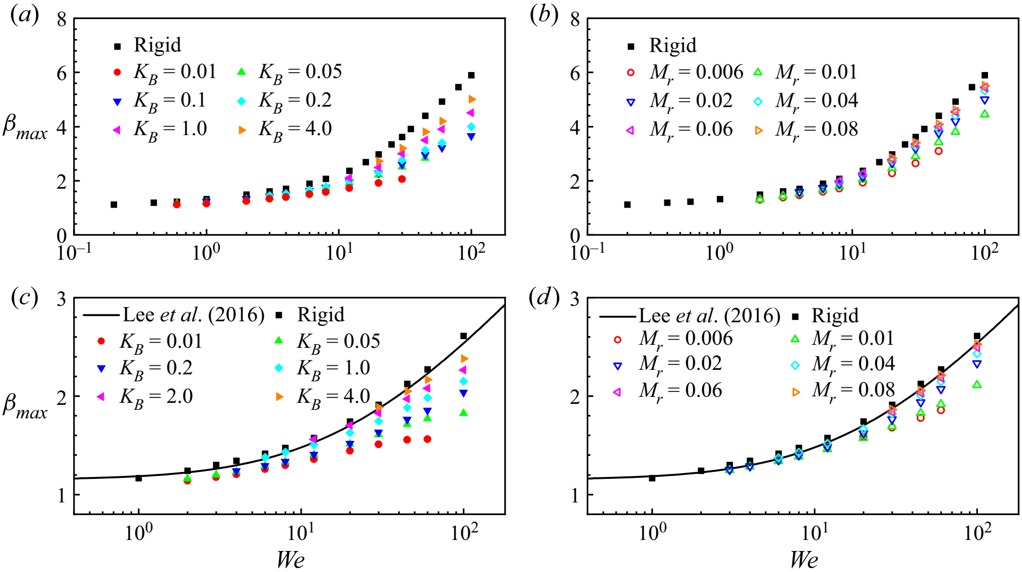

Figure 4. The maximum spreading ratio β_{max} as a function of We for cases with different K_B but identical $M_r = 0.01$ (*a*,*c*), and different M_r but identical $K_B = 0.6$ (*b*,*d*). (*a*,*b*) Two-dimensional cases. (*c*,*d*) Three-dimensional cases. The solid curves represent the universal rescalings of Lee *et al.* (2016) for rigid cases.

is infinite. Second, in both 2-D and 3-D cases, chordwise bending is dominant because only two chordwise ends of the plate are supported in the 3-D cases. Third, there is no spanwise bending and stretching of the plate in 2-D cases. The spanwise bending and stretching are also very minor in 3-D simulations because in the spanwise direction, i.e. the y direction in figure 1(*b*), both sides of the plate are free.

3.1. *Evolutions of droplet spreading and energies*

In order to understand the effect of the flexible substrate on droplet spreading, figure 5 shows snapshots of the impacting droplet at $We = 30$ and $M_r = 0.01$ with four different K_B values of 0.05, 0.6, 4.0 and ∞ (the rigid case). Once the droplet contacts the substrate ($t = 0.04$), the flexible plate begins to move downwards. In all cases, all lamellas begin to move outwards. At $t = 0.15$, we can see that there are rims in all cases. Besides, the more flexible the plate is, the smaller the spreading diameter. This indicates a lower averaged spreading speed in the case with a more flexible plate. However, in all cases the spreading diameters reach their peaks D_{max} at approximately $t = 0.45$. Hence, the flexible substrate has little effect on the maximum spreading time t_{max} ($t \approx 0.45$), which is consistent with the observation in the experimental study of Vasileiou *et al.* (2016).

Here, we would like to discuss some details at $t = t_{max}$. Figure 5 shows that at $t = t_{max}$ spreading reaches D_{max} when the plate is moving downwards to its maximum deflection d_{max} for small K_B, e.g. cases (*c*,*d*). These cases are referred to as 'early spreading cases'. However, if K_B is relatively large, e.g. case (*b*) with $K_B = 4.0$, the oscillation frequency of the substrate is high enough, and upwards deflection of the substrate before t_{max} may appear. It is referred to as the 'delayed spreading case' (see the caption of figure 5). In the delayed spreading case (figure 5*b*), a part of momentum or energy is returned to the droplet through the substrate's upwards motion, which results in a slight lifting up of the

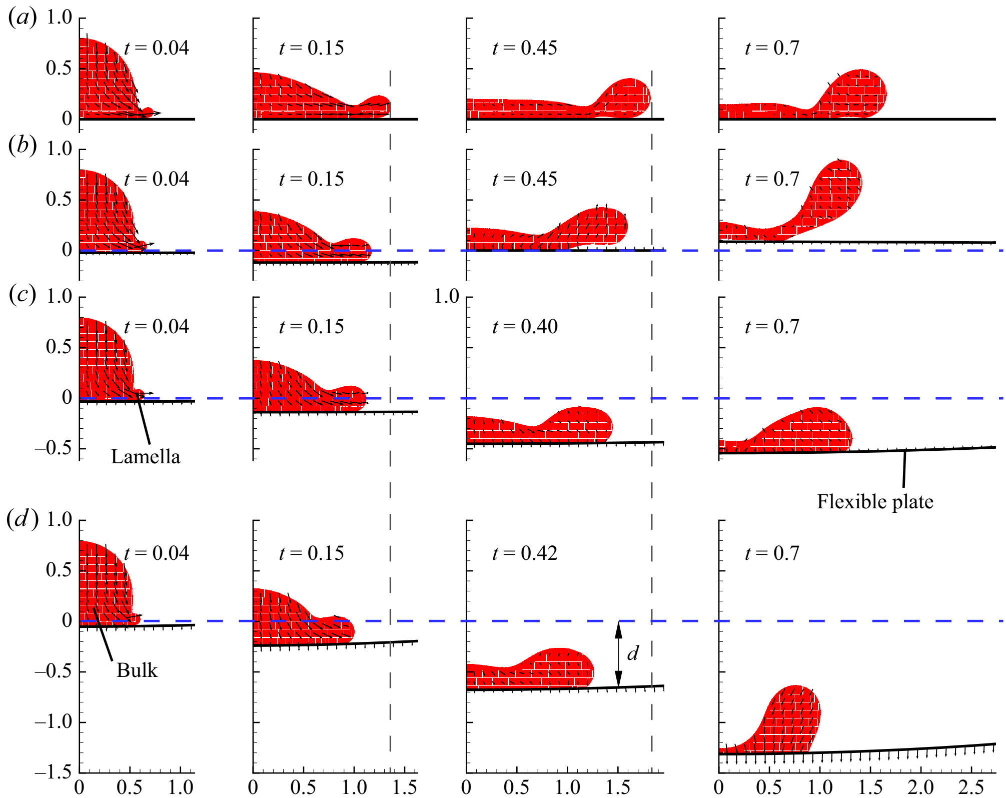

Figure 5. Snapshots of an impacting droplet for rigid and flexible cases (two dimensional) at $We = 30$, $M_r = 0.01$ with different K_B: (*a*) rigid ($K_B = \infty$), (*b*) $K_B = 4.0$, (*c*) $K_B = 0.6$ and (*d*) $K_B = 0.05$. Four typical moments (four columns) $t = 0.04$, 0.15, t_{max} and 0.7 are chosen. Here, t_{max} is the moment when the maximum spreading occurs. The blue dotted lines denote the initial locations of the flexible plate. (*d*) Vertical deflection of the plate. In case (*b*), the spreading reaches D_{max} after the plate's maximum deflection is achieved, namely, the delayed spreading case. In cases (*c*,*d*), the spreading reaches D_{max} before that, namely, early spreading cases.

rim at the maximum spreading. This rising at $t = 0.7$ is more obvious because the flexible substrate begins to move downwards again at this moment. The attached droplet also moves downwards, while the edge of the droplet still moves upwards, thus intensifying the rise of the rim. For cases (*c*,*d*) ($K_B = 0.6$ and 0.05), because the flexible plate keeps a downwards movement during the droplet spreading, there is no rising rim.

Here, by the way, we would like to justify the parameter ranges in our study. From figure 5 we can see that in all cases any local segment of the plate is almost flat. This is the main characteristic of the cases that we investigated, i.e. the spreading of the droplet is not confined by the curvature effect of the plate. In this study we only focus on cases of this kind. On the other hand, when K_B and M_r are small enough or We is large enough, the impact on the flexible plate is more prominent. Furthermore, the local segment of the plate contacting the droplet may deform severely, which looks like a shallow well (see figure 6). Figure 6 shows a 2-D example with $K_B = 0.01$, $M_r = 0.01$ and $We = 100$. In this case the rim of the well significantly confines the spreading of the droplet. Therefore, the flow regime would be significantly different from that in the present study. Since we are only interested in cases without confinement due to curvature, here we do not consider

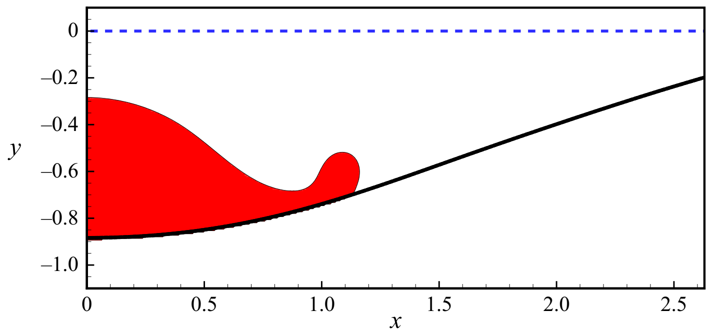

Figure 6. Local zoom-in view of a droplet impacting on the flexible plate with $We = 100$, $K_B = 0.01$ and $M_r = 0.01$ at $t = 0.2$. The blue dotted line denotes the initial location of the flexible plate.

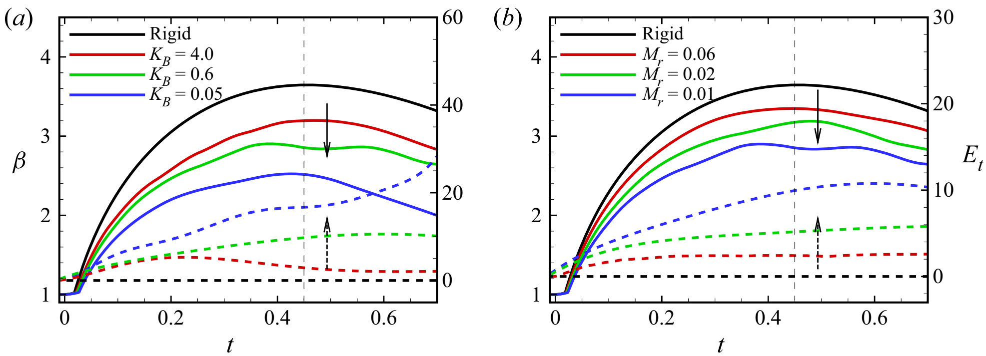

Figure 7. The time evolution of β (solid lines) and the total energy of plates E_t (dotted lines) for rigid and flexible cases at $We = 30$ with (*a*) different K_B ($M_r = 0.01$ is fixed), (*b*) different M_r ($K_B = 0.6$ is fixed). The arrows point in the direction that K_B or M_r decreases. Here, E_t contains the elastic and kinetic energies of the plate, which is zero for rigid cases.

the cases with higher Weber numbers, i.e. $We > 100$. For the same reason, $K_B < 0.01$ and $M_r < 0.006$ are not taken into account.

In the following, from the energy viewpoint, we explain why β_{max} decreases as K_B or M_r decreases as shown in figure 7. For the rigid case, the initial kinetic energy E_k of the droplet is mainly converted into the surface energy at the maximum spreading. While, for flexible cases, part of the initial kinetic energy is converted into the elastic and kinetic energies of the plate, therefore, less energy is available for spreading, which results in a smaller D_{max}. Figure 7(*a*) shows the evolution of the spreading ratio β and the total energy E_t of the plate for cases in figure 5. We can see that at t_{max} ($t \approx 0.45$), E_t increases as K_B decreases. Therefore, at t_{max}, more initial energy is transferred to the plate if it is more flexible. Besides, in the cases of different M_r but fixed K_B (see figure 7*b*), at t_{max} ($t \approx 0.45$), E_t increases as M_r decreases. It is reasonable because if the plate is lighter (smaller M_r), the impact seems more significant, and more kinetic energy would pass to the plate. Therefore, β_{max} decreases as K_B or M_r decreases, and is always smaller than rigid cases with the same We.

In the analysis of energy conversion, the role of viscous dissipation should also be discussed. On the one hand, a more flexible substrate implies that more initial kinetic energy of the drop goes into the substrate. On the other hand, a more flexible substrate also suggests that the inertial shock during impact is mitigated. Consequently, the viscous

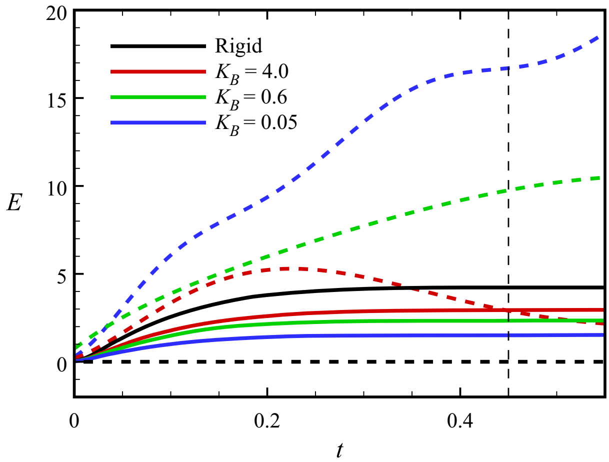

Figure 8. The time evolution of viscous dissipation (solid lines) and the total energy of substrates (dotted lines are identical to those in figure 7*a*) in cases of $We = 30$, $M_r = 0.01$ but different K_B (two dimensional). The viscous dissipation is calculated as $\mu_H(\partial u/\partial y)^2$ (Wildeman *et al.* 2016). The droplet reaches the maximum spreading at $t_{max} = 0.45$.

dissipation inside the drop would decrease (due to smaller velocity gradients). This point is confirmed through our following tests. We carried out several simulations with $We = 30$, $M_r = 0.01$ but different K_B. The evolution of viscous dissipation and the total energy of substrates are shown in figure 8. We can see that the viscous dissipation decreases as the stiffness K_B decreases.

Generally speaking, less viscous dissipation implies more surface energy of the droplet, which is favourable for droplet spreading. However, we can also see that when K_B changes, compared with the energy of the substrate, the viscous dissipation only changes in a very limited range and is minor. Therefore, the effect of viscous dissipation is very minor compared with the energy loss (absorbed by the substrates). Therefore, a more flexible substrate still leads to less surface energy (at t_{max}). The viscous dissipation does not affect the conclusion that the β_{max} decreases as K_B or M_r decreases.

3.2. *Rescaling the acceleration during impact*

During impact, the droplet experiences a force exerted by the solid wall, which decelerates the droplet. According to Clanet *et al.* (2004), the initial velocity U_0 of the droplet decreases to 0 at the maximum spreading along with a displacement of D_0 (rigid case in figure 2*a*) and, thus, the average acceleration a during this process can be scaled as $a \sim U_0^2/D_0$. It is noted that Ye & Van Der Meer (2021) also got the same acceleration from the viewpoint of energy, considering this force being equal to the impact kinetic energy divided by the displacement. However, when the same droplet impacts the flexible substrate, its downwards movement leads to a larger displacement during the decelerating process as shown in figure 2. As a consequence, the average acceleration a is reduced. It can be regarded that the droplet impacts the rigid surface with a lower initial velocity (Ye & Van Der Meer 2021). We can understand this from figure 2 in which, for the flexible case, the droplet impacts the same surface as the rigid cases in a lower We, leading to a reduction of the maximum spreading diameter.

Vasileiou *et al.* (2016) scaled the average acceleration of droplets impacting on flexible substrates as

$$a \approx U_0^2/[D_0(1 + m_d/m_b)], \tag{3.1}$$

considering the momentum conservation between the droplet and the substrate, where m_d and m_b are their masses, respectively. It can only characterize the cases of different mass ratios but the stiffness effect is not considered. In other words, it is no longer applicable when K_B changes.

However, as we have seen from our simulation results, the stiffness K_B can also significantly affect the maximum spreading. Moreover, Vasileiou *et al.* (2016) only considered the early spreading cases (small K_B, low vibration frequency) instead of the delayed spreading cases (large K_B), i.e. the spreading reaches D_{max} after the plate's maximum deflection is achieved (see figure 5). Therefore, (3.1) is no longer applicable with a high K_B or low M_r, which leads to a high vibration frequency in our simulation.

Here, we propose to rescale the average acceleration a for flexible substrates in the following way. As mentioned above, compared with the rigid case, the droplet impacting on flexible substrates travels a larger displacement during the deceleration process (see figure 2). Here, the total displacement scales as the sum of the initial droplet diameter and the maximum deflection of the flexible substrate, namely $D_0 + d_{max}$. So the average acceleration can be rescaled as

$$a \sim U_0^2/(D_0 + d_{max}), \tag{3.2}$$

where d_{max} contains the effects of both K_B and M_r, as can be seen in (3.4).

In the following we would like to verify the rescaled average acceleration from the point of view of the energy. From the analysis above, we can see that compared with $a \sim U_0^2/D_0$ for rigid cases, there is a smaller acceleration $a \sim U_0^2/(D_0 + d_{max})$ in the flexible cases. We can imagine in terms of acceleration that the flexible case with velocity U_0 is equivalent to the rigid case with velocity $U_0\sqrt{D_0/(D_0 + d_{max})}$. Therefore, in the flexible case with U_0, the actual kinetic energy that is used for spreading to the maximum diameter is $E_{s,max} \approx E_k D_0/(D_0 + d_{max})$, where E_k is the initial kinetic energy. The remaining energy is supposed to be used for the deformation and motion of substrates, i.e. $E_{t,max} = E_k - E_{s,max} \approx E_k d_{max}/(D_0 + d_{max})$, as discussed in § 3.1.

Figure 9(*a*) shows the total energy of the substrate at the maximum spreading $E_{t,max}$ as a function of the initial kinetic energy E_k for the cases with different K_B or M_r. We can see that all the numerical data are below the black line $E_{t,max} = E_k$. This indicates that $E_{t,max} < E_k$, i.e. only part of E_k is converted into $E_{t,max}$. To verify $E_{t,max} \approx E_k d_{max}/(D_0 + d_{max})$, we change the coordinate of E_k to $E_k d_{max}/(D_0 + d_{max})$. The result is shown in figure 9(*b*), in which all the data points are around the black line, i.e. $E_{t,max} = E_k d_{max}/(D_0 + d_{max})$. It is noted that even for the delayed spreading cases ($K_B = 4.0$ and 1.0 in figure 9), the results also agree well. Therefore, all of our data that come from cases with different K_B or M_r support the formula $E_{t,max} \approx E_k d_{max}/(D_0 + d_{max})$. Since the formula is derived from (3.2), we confirm that all of our data support the rescaled acceleration.

3.3. *Scaling law*

In this section we aim to seek a nice data collapse by introducing an effective Weber number We_m, which accounts for the substrate properties without any adjustable parameters. The aim is achieved by the energy analysis discussed in § 3.2.

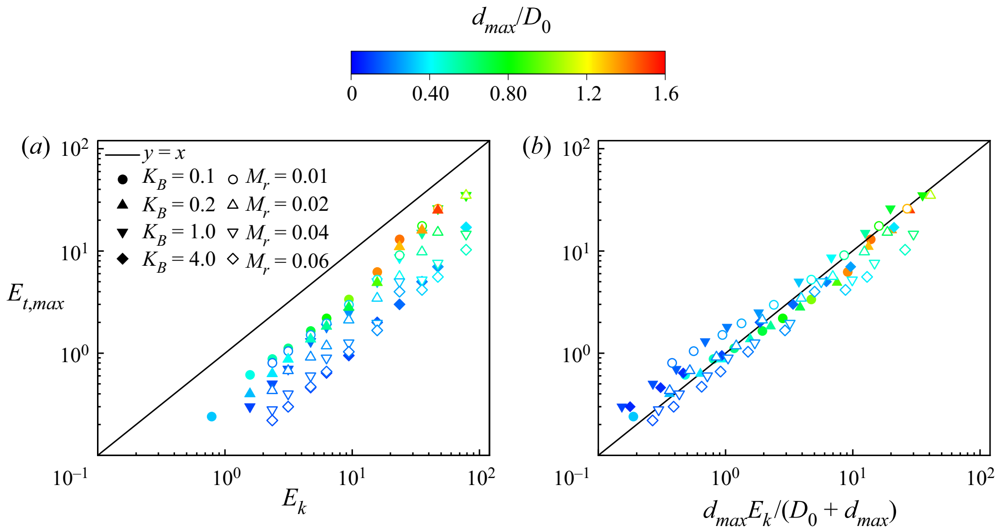

Figure 9. The total energy of plates at the maximum spreading $E_{t,max}$ as a function of (*a*) the initial kinetic energy E_k; and (*b*) $d_{max}E_k/(D_0 + d_{max})$ for cases with different K_B but a fixed $M_r = 0.01$ (filled symbols), and those with different M_r but a fixed $K_B = 0.6$ (open symbols). The solid black lines denote $E_{t,max} = E_k$ and $E_{t,max} = d_{max}E_k/(D_0 + d_{max})$ in (*a*,*b*), respectively. The colour of the symbols indicates the dimensionless maximum deflection of the plate d_{max}/D_0. Here, $E_{t,max}$ and d_{max} are obtained through our numerical simulations (see the details of $E_{t,max}$ in figure 7).

Furthermore, another effective Weber number We_e directly derived from energy conservation confirms the validation of the scaling law.

From the above analysis, we know that in the flexible cases only a part of the kinetic energy (characterized by U_0^2 or We) contributes to the spreading of the droplet. Here, an effective Weber number We_m is defined to characterize the contribution. Since part of the initial kinetic energy, $E_kD_0/(D_0 + d_{max})$ is available for spreading, we can define the effective Weber number as

$$We_m = \frac{WeD_0}{D_0 + d_{max}} = \frac{We}{1 + \delta_{max}}, \tag{3.3}$$

where $\delta_{max} = d_{max}/D_0$. To get the theoretical We_m, we have to theoretically determine d_{max} first. Actually, the d_{max} can also be obtained by the momentum conservation (Soto *et al.* 2014) as follows. The initial momentum p_0 of the droplet is mU_0, where m is the mass of the droplet. After impact, the droplet and the flexible substrate vibrate together. According to Soto *et al.* (2014), when the droplet impacts the flexible substrate, the centre of the substrate obtains a velocity $U_M = 2\pi f d_{max}$, where $f = f_0[M_s/(m + M_s)]^{1/2}$ is the vibration frequency of the system, M_s the mass of the flexible substrate and f_0 the natural vibration frequency of the flexible substrate. For a simple-support plate on both ends, we have $f_0 = \pi\sqrt{EI_M/M_sL^3}/2$ by the Euler–Bernoulli beam theory, where $I_M = h_s^3W/12$ is the second moment of inertia (W is the width of the plate and is set to unity in 2-D cases). Furthermore, according to Soto *et al.* (2014), the plate vibrates with a parabolic shape and its momentum can be written as $p_M = 2\int_0^{L/2} \rho_s Wh_sU_Mx^2/L^2\,\mathrm{d}x = M_sU_M/3$. Meanwhile, the momentum of the droplet vibrating at the centre of the substrate is $p_m = mU_M$. Due to

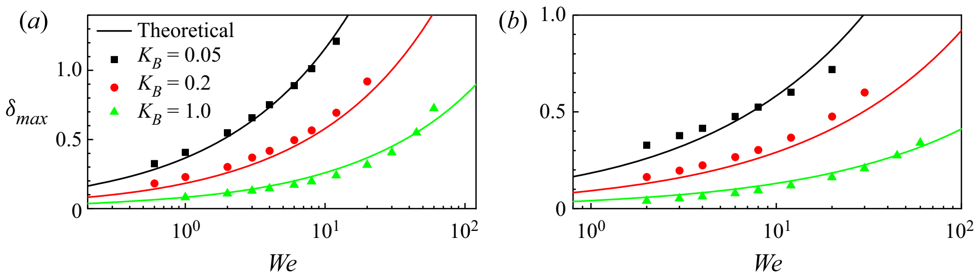

Figure 10. The δ_{max} as a function of We for the (a) 2-D and (b) 3-D cases of different K_B ($M_r = 0.01$). The symbols represent the numerical results. The solid curve denotes the prediction of (3.4).

momentum conservation, we have $p_0 = p_M + p_m$. Therefore, d_{max} can be predicted as

$$d_{max} = \frac{1}{2\pi}\frac{m}{m + M_s/3}\frac{U_0}{f}. \tag{3.4}$$

Figure 10 shows that the numerical results of δ_{max} as a function of We are in good agreement with the prediction of (3.4) for both 2-D and 3-D cases, which supports the above derivation.

In the above, we can see that the effective Weber number We_m takes all the factors (We, K_B and M_r) affecting β_{max} into account. When K_B or M_r is large enough (close to the rigid case), $\delta_{max} \to 0$, we have $We_m \to We$. The theoretical We_m values for all cases in figure 4 can be obtained through (3.3) and (3.4). Figure 11(a,b) shows the numerical 2-D and 3-D results of β_{max} as a function of We_m, respectively. We can see that through We_m all 2-D and 3-D data almost collapse onto a single curve, respectively. Furthermore, the single curve for 3-D cases can be well represented by the universal rescaling proposed by Lee *et al.* (2016).

Besides our proposed scaling of (3.3), another similar scaling based on momentum conservation is available for different situations in the literature, i.e. $We_m = We/(1 + m_d/m_b)$ (Vasileiou *et al.* 2016), where m_d and m_b are the masses of the droplet and plate, respectively. Figure 11(d) shows a comparison between different scalings. The blue and red symbols in figure 11(d) represent normalized data for flexible cases using our scaling of (3.3) and Vasileiou *et al.* (2016), respectively. The black symbols are normalized data for rigid cases, in which $We_m = We$. It is noted that the original data (Vasileiou *et al.* 2016) are shown in figure 11(c). It is seen that through our scaling, all data collapse onto a single curve.

From figure 11(d) it can be seen that Vasileiou *et al.* (2016) can indeed correctly predict the maximum spreading diameter of the droplet impacting flexible substrates with the acceleration term of (3.1), even neglecting the change of the stiffness. However, this is attributed to the low natural frequency of flexible substrates, i.e. very flexible substrates. Since their substrates are very flexible, the assumption of a perfectly inelastic collision between the droplet and the substrates is valid. Under this assumption, they accurately obtained the initial velocity of the plate after impacting, then got the acceleration term correctly. Therefore, in their cases, they can neglect stiffness. However, when the stiffness is relatively large, the assumption of perfectly inelastic collision is no longer valid, and the acceleration term of (3.1) obtained by them is not applicable. While our derived acceleration is suitable for both large and small stiffnesses (figure 11a,b). Moreover, we can also get accurate theoretical predictions with the same stiffness as Vasileiou *et al.* (2016) (figure 11d).

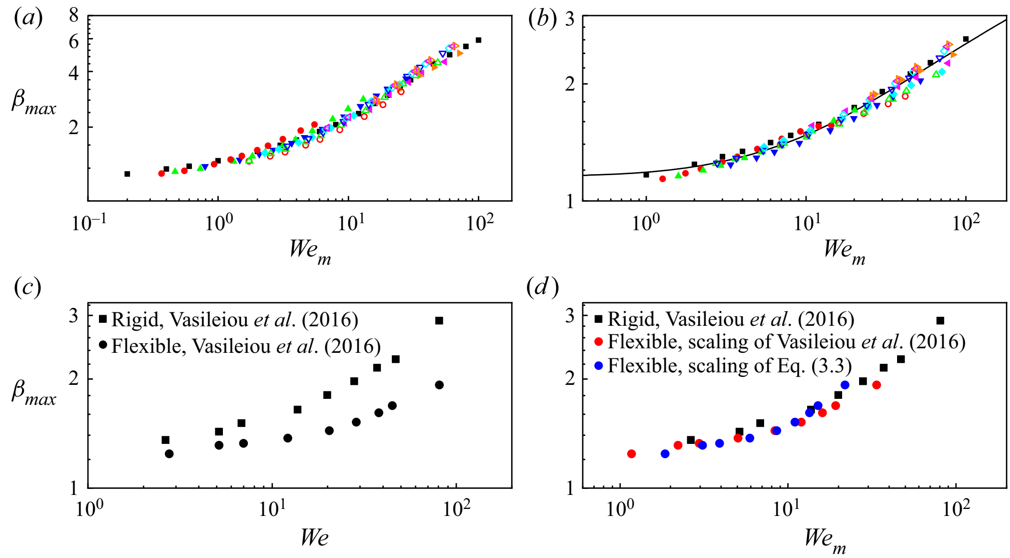

Figure 11. The maximum spreading ratio β_{max} as a function of We_m in the (*a*) 2-D and (*b*) 3-D cases, where all symbols come from figure 4. The solid line is the scaling of Lee *et al.* (2016) for rigid cases. (*c*) Original experimental data (β_{max} as a function of We) for rigid and flexible cases in Vasileiou *et al.* (2016). (*d*) Plot of β_{max} vs We_m (data are identical to those in *c*). For black squares (rigid cases), $We_m = We$. For the red disks, $We_m = We/(1 + m_d/m_b)$ (Vasileiou *et al.* 2016). For the blue disks, We_m is obtained through (3.3) and (3.4).

In the following, we validate the scaling (3.3) through another effective Weber number We_e, which is directly derived from energy conservation. From the analysis above, we know that for flexible substrates, the initial kinetic energy E_k is converted into E_s and E_t, i.e. $E_k = E_s + E_t$, and only E_s contributes to the spreading. Suppose We_e is proportional to the energy used for maximum spreading $E_{s,max}$, we have

$$We_e = We\frac{E_{s,max}}{E_k} = We\left(1 - \frac{E_{t,max}}{E_k}\right). \tag{3.5}$$

On the other hand, from § 3.2 we know that $E_{s,max} \approx E_k D_0/(D_0 + d_{max})$. Substituting it into (3.5), we have $We_e \approx WeD_0/(D_0 + d_{max})$, which is almost identical to We_m. Although $We_e \approx We_m$, here We_e (3.5) is *a posteriori* since $E_{t,max}$ has to be determined by numerical results, e.g. the data in figure 9. After We_e's for all the cases in figure 4 are obtained, we can plot the maximum spreading ratio β_{max} as a function of We_e for all cases (see figure 12). We can see that all 2-D data almost collapse onto a single curve (figure 12*a*), so do the 3-D data (figure 12*b*). Furthermore, the single curve can also be well represented by the scaling of Lee *et al.* (2016).

In summary, figures 11(*b*) and 12(*b*) show that We_m and We_e formulas all lead to nice data collapses, which are all consistent with the scaling of Lee *et al.* (2016). It is noted that our proposed theoretical We_m is *a priori*, and there are no adjustable parameters, while We_e is *a posteriori* energy analysis that does confirm the validation of our *a priori* scaling law.

4. Conclusion

We have numerically simulated the droplet impacting on the flexible plate, and investigated the effect of the flexible substrate on the maximum spreading ratio β_{max} for different K_B

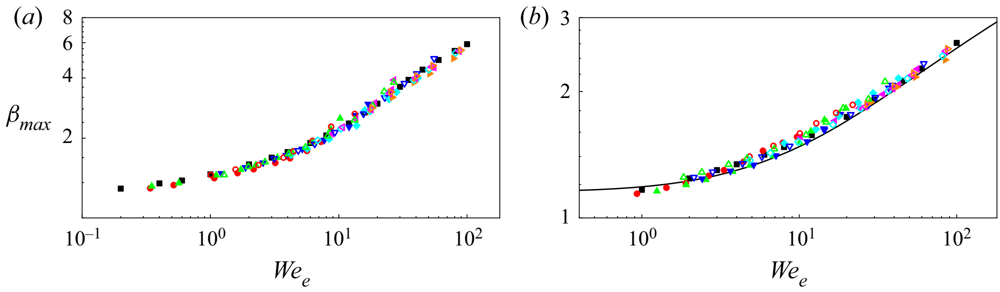

Figure 12. The maximum spreading ratio β_{max} as a function of We_e in the (*a*) 2-D and (*b*) 3-D cases, where all symbols come from figure 4. The solid line denotes the scaling of Lee *et al.* (2016) for rigid cases.

($K_B \in [0.01, \infty)$) and M_r ($M_r \in [0.006, \infty)$) in a wide range of We ($We \in [0.1, 100]$). Our study is limited to the cases in which droplet spreading is not affected by the substrate curvature. We observed that β_{max} is reduced compared with the rigid case because partial initial energy is passed to the flexible plate, and less energy is available for spreading. Based on the energy analysis, we demonstrated that the vertical movement of the flexible substrate reduces the average acceleration a during spreading, which can be regarded as the droplet impacting with less initial kinetic energy, leading to a decrease of the D_{max}. Furthermore, we theoretically derived an effective We_m, through which nice data collapses can be achieved. The scaling is also supported by an *a posteriori* energy analysis. Therefore, we successfully proposed a scaling of β_{max} for droplets impacting flexible substrates (including the rigid cases) over a wide range of We.

Funding. This work was supported by the National Science Foundation of China (NSFC) (grant nos. 11772326 and 11972342).

Declaration of interests. The authors report no conflict of interest.

Author ORCIDs.
Yufei Ma https://orcid.org/0000-0001-5489-1302;
Haibo Huang https://orcid.org/0000-0002-1308-9900.

References

Bergeron, V., Bonn, D., Martin, J.Y. & Vovelle, L. 2000 Controlling droplet deposition with polymer additives. *Nature* **405** (6788), 772–775.

Clanet, C., Béguin, C., Richard, D. & Quéré, D. 2004 Maximal deformation of an impacting drop. *J. Fluid Mech.* **517**, 199–208.

Derby, B. 2010 Inkjet printing of functional and structural materials: fluid property requirements, feature stability, and resolution. *Annu. Rev. Mater. Res.* **40**, 395–414.

Dorschner, B., Chikatamarla, S.S. & Karlin, I.V. 2018 Fluid-structure interaction with the entropic lattice Boltzmann method. *Phys. Rev.* E **97** (2), 023305.

Doyle, J.F. 2001 *Nonlinear Analysis of Thin-Walled Structures: Statics, Dynamics, and Stability*. Springer Science & Business Media.

Eggers, J., Fontelos, M.A., Josserand, C. & Zaleski, S. 2010 Drop dynamics after impact on a solid wall: theory and simulations. *Phys. Fluids* **22** (6), 062101.

Fakhari, A. & Bolster, D. 2017 Diffuse interface modeling of three-phase contact line dynamics on curved boundaries: a lattice Boltzmann model for large density and viscosity ratios. *J. Comput. Phys.* **334**, 620–638.

Gart, S., Mates, J.E., Megaridis, C.M. & Jung, S. 2015 Droplet impacting a cantilever: a leaf-raindrop system. *Phys. Rev. Appl.* **3** (4), 044019.

Howland, C.J., Antkowiak, A., Castrejón-Pita, J.R., Howison, S.D., Oliver, J.M., Style, R.W. & Castrejón-Pita, A.A. 2016 It's harder to splash on soft solids. *Phys. Rev. Lett.* **117** (18), 184502.

Hua, R.N., Zhu, L.D. & Lu, X.Y. 2014 Dynamics of fluid flow over a circular flexible plate. *J. Fluid Mech.* **759**, 56–72.

Josserand, C. & Thoroddsen, S.T. 2016 Drop impact on a solid surface. *Annu. Rev. Fluid Mech.* **48**, 365–391.

Joung, Y.S. & Buie, C.R. 2015 Aerosol generation by raindrop impact on soil. *Nat. Commun.* **6** (1), 1–9.

Kim, S., Wu, Z., Esmaili, E., Dombroskie, J.J. & Jung, S. 2020 How a raindrop gets shattered on biological surfaces. *Proc. Natl Acad. Sci. USA* **117** (25), 13901–13907.

Laan, N., de Bruin, K.G., Bartolo, D., Josserand, C. & Bonn, D. 2014 Maximum diameter of impacting liquid droplets. *Phys. Rev. Appl.* **2** (4), 044018.

Lee, J.B., Laan, N., de Bruin, K.G., Skantzaris, G., Shahidzadeh, N., Derome, D., Carmeliet, J. & Bonn, D. 2016 Universal rescaling of drop impact on smooth and rough surfaces. *J. Fluid Mech.* **786**, R4.

Liang, H., Xu, J.R., Chen, J.X., Wang, H.L., Chai, Z.H. & Shi, B.C. 2018 Phase-field-based lattice Boltzmann modeling of large-density-ratio two-phase flows. *Phys. Rev.* E **97** (3), 033309.

Pan, J.-H., Ni, M.-J. & Zhang, N.-M. 2018 A consistent and conservative immersed boundary method for MHD flows and moving boundary problems. *J. Comput. Phys.* **373**, 425–445.

Pasandideh-Fard, M., Qiao, Y., Chandra, S. & Mostaghimi, J. 1996 Capillary effects during droplet impact on a solid surface. *Phys. Fluids* **8** (3), 650–659.

Pegg, M., Purvis, R. & Korobkin, A. 2018 Droplet impact onto an elastic plate: a new mechanism for splashing. *J. Fluid Mech.* **839**, 561–593.

Roisman, I.V. 2009 Inertia dominated drop collisions. II. An analytical solution of the Navier–Stokes equations for a spreading viscous film. *Phys. Fluids* **21** (5), 052104.

Shao, J.Y., Shu, C. & Chew, Y.-T. 2013 Development of an immersed boundary-phase field-lattice Boltzmann method for Neumann boundary condition to study contact line dynamics. *J. Comput. Phys.* **234**, 8–32.

Soto, D., De Lariviere, A.B., Boutillon, X., Clanet, C. & Quéré, D. 2014 The force of impacting rain. *Soft Matt.* **10** (27), 4929–4934.

Vasileiou, T., Gerber, J., Prautzsch, J., Schutzius, T.M. & Poulikakos, D. 2016 Superhydrophobicity enhancement through substrate flexibility. *Proc. Natl Acad. Sci. USA* **113** (47), 13307–13312.

Wang, Y.F., Wang, Y.B., He, X., Zhang, B.X., Yang, Y.R., Wang, X.D. & Lee, D.J. 2022 Scaling laws of the maximum spreading factor for impact of nanodroplets on solid surfaces. *J. Fluid Mech.* **937**, A12.

Weisensee, P.B., Tian, J., Miljkovic, N. & King, W.P. 2016 Water droplet impact on elastic superhydrophobic surfaces. *Sci. Rep.* **6** (1), 1–9.

Wildeman, S., Visser, C.W., Sun, C. & Lohse, D. 2016 On the spreading of impacting drops. *J. Fluid Mech.* **805**, 636–655.

Xiong, Y.F., Huang, H.B. & Lu, X.Y. 2020 Numerical study of droplet impact on a flexible substrate. *Phys. Rev.* E **101** (5), 053107.

Ye, X. & Van Der Meer, D. 2021 Hydrogel sphere impact cratering, spreading and bouncing on granular media. *J. Fluid Mech.* **929**, A24.